

MOONRAY: A permanent high-energy cosmic-ray observatory on the surface of the Moon

P.S. Marrocchesi *

Department of Physical Sciences, Earth and Environment, University of Siena, V. Roma 56, 53100 Siena, Italy
INFN sez. di Pisa, Largo B. Pontecorvo 3, 56127 Pisa, Italy

ARTICLE INFO

Keywords:

Cosmic-ray
Lunar telescope

ABSTRACT

The forthcoming decades will see a rapid development of space programs aiming at the implementation of habitats on our satellite. Therefore it makes sense to evaluate the feasibility of a permanent cosmic-ray (CR) observatory on the Moon. Its large sensitive area would allow to carry out a very rich observational program over a time span of a few decades with an unprecedented energy reach. A thorough exploration of the energy region around the CR spectral anomaly located at a few PeV, also known as the “knee”, will become possible.

In this paper we propose an innovative concept of a *modular* lunar observatory designed to overcome the limitations of the present generation of cosmic-ray telescopes in Low Earth Orbit. It consists of an array of fully independent modules with limited individual size and weight. This would allow an ample flexibility in the gradual deployment of a progressively larger active volume, while ensuring the collection of meaningful scientific data during the intermediate stages of its implementation. Each independent module consists of three main instruments: a combined Charge and Time-of-Flight detector to identify individual elements from proton to nickel (and beyond), a tracker providing the direction and impact point of the incident particle, and a calorimeter to measure its kinetic energy. The design of each instrument contains innovative solutions that are well within the reach of the present technology.

1. Introduction

The last decade has been marked by the discovery of unexpected features in the energy spectra of charged cosmic rays (Refs. [1–9]). In particular, significant deviations of the fluxes from a pure power-law spectrum have been observed by CREAM [10], PAMELA [11], AMS-02 [12], CALET [13], and DAMPE [14]. Direct measurements have also shown that the rigidity dependence of primary and secondary cosmic elements is different [15]. A recent unexpected discovery was the observation of a flattening in the rigidity of the proton and helium spectra. Starting from a few hundred GeV, the proton flux shows a smooth and progressive “hardening” of the spectrum that continues up to ~ 10 TeV, above which a completely different regime is established. A turning point was the subsequent discovery of an unexpected “softening” of proton and helium fluxes at the multi-TeV scale (CALET, DAMPE). These anomalies, that encode information about cosmic-ray acceleration processes and on the history of their propagation in the Galaxy, have given rise to a large variety of theoretical interpretations. The two spectral features might result from a single physical process that generates a sort of “bump” in the CR spectrum (between a few hundred GeV/n to about 50 TeV/n) or from a more complex astrophysical scenario. The emergence of this new rich phenomenology is

being addressed by several theoretical models (Refs. [16–31]) in the quest for a consistent picture of cosmic-ray phenomena. They include: the possibility of an anomalous diffusive regime near the acceleration sources; the dominance of one (or more) nearby supernova remnant(s) (SNR) in the framework of specific models of confinement and gradual release of CRs from the source; the presence of additional sources. The discovery of a second break challenges the conventional interpretations of CR spectra described earlier and calls for an extension of the observations to PeV energies. The experimental challenge for the years to come is to reach even higher energies and explore the “knee” (approximately one decade around 3–4 PeV), a third spectral anomaly discovered more than half a century ago in the all-particle cosmic ray flux. Characterized by a broken power-law with a spectral index increasing from ~ 2.7 below 10^{14} eV to ~ 3.1 above 10^{16} eV, the “knee” has been driving the efforts of generations of researchers for decades.

At present, only two experiments in Low Earth Orbit (LEO) have a sufficient energy reach to extend the range of direct measurements above 100 TeV (CALET and DAMPE). They rely on a purely calorimetric measurement of the energy, while space-borne magnetic spectrometers are limited to a maximum magnetic rigidity (MDR) of a few TVs. After

* Correspondence to: Department of Physical Sciences, Earth and Environment, University of Siena, V. Roma 56, 53100 Siena, Italy.
E-mail address: marrocchesi@unisi.it.

the end of PAMELA operations, AMS-02 is the only instrument in orbit with the ability to discriminate the sign of the charge. This allows to carry out separate measurements of the high-energy spectra of positrons and anti-protons, an important input to the observation of final states containing anti-particles for the search of Dark Matter.

The calorimetric instruments in operation at this time, though capable of measuring single-particle energies up to the PeV scale, are unable to provide statistically relevant information on the region from 10^{15} eV to 10^{16} eV due to the dramatic reduction of the fluxes with increasing energy (about a factor of 50 per decade) and to their limited size, constrained by the available maximum weight and power. These two well-known limitations of instruments operating in space make it problematic to build a large area telescope with sufficient collecting power to accumulate, in a reasonable mission timescale (10–15 years), the statistics needed to study the energy interval around the “knee”.

In order to address this challenge, an experimental apparatus is required to have a geometric acceptance of at least $3 \text{ m}^2\text{sr}$, i.e., more than one order of magnitude larger than the space instruments in flight at present. A similar goal is being pursued by a large-acceptance payload (HERD) designed to carry out a campaign of observations aboard the Chinese Space Station with a time span possibly extending beyond the end of the present decade. On an even longer time scale, two large missions, AMS100 [32] and ALADiO [33], have been proposed for long-term observations in a stable orbit around the Lagrangian point L2.

The basic idea of the MOONRAY project is the key to the sustainability of its implementation: the design of a *modular* telescope that can be installed progressively, over consecutive lunar missions, until the required geometric acceptance is achieved. This requires the implementation of some innovative ideas on the development of the experimental apparatus, yet remaining within the framework of technologies that are already available. One of the two major advantages of a large CR telescope operating on the Moon is the availability of a larger electric power to operate the electronics with respect to an orbital instrument, which is typically limited to a few kW. Indeed, sufficient power will be made available by the installations that will be built on the lunar surface and that will have to be functional for the sustainability of the habitat. A second advantage is the low lunar gravity (about 1/6 than on Earth), which would facilitate the installation of modules of reasonable size and weight. The study of a modular apparatus designed to carry out direct observations of high-energy charged cosmic radiation (from proton to trans-Fe elements with atomic number $Z \leq 40$) operating on the Moon and of the innovative detectors necessary for its implementation are briefly described in the following section.

2. Innovative concepts for a modular cosmic-ray telescope

The MOONRAY main instrument is structured into vertical units called “towers” (Fig. 1). Each tower is a completely independent functional unit. The sensitive area of the telescope is extended during consecutive missions with the deployment of extra towers, while keeping the instrument operational in between two subsequent phases of the upgrade of the instrument. This approach differs markedly from that used on current orbital missions, whereby the experimental apparatus is assembled on the ground before launch and its maximum geometric acceptance is fixed and heavily penalized by weight and power limitations.

The MOONRAY design relies on a set of highly innovative ideas in high-energy particle instrumentation. Each tower includes three main instruments:

- a particle identifier (CD-ToF), integrating high resolution Time-of-Flight (ToF) capabilities into a charge detector (CD), for the simultaneous measurement of the electric charge and time of arrival of the incident particle. This is a newly developed instrument based on Low Gain Avalanche Diodes (LGAD) sensors with sub-ns time resolution. It

allows a clean charge identification of the CR incident particle thanks to an efficient rejection of the copious back-scattering background generated by its interaction with the calorimeter;

- a modular tracking system (MoonTracker or MT) based on semiconductor position detectors or, alternatively, on a scintillating fiber tracker with silicon photodetectors (SiPM) readout;
- a homogeneous calorimeter (MCAL) based on integrated modules of reasonable size and weight, each consisting of a 3D array of scintillating crystals readout by photodiodes.

2.1. The CD-ToF particle identifier

As it is well known, calorimetric instruments suffer from the presence of backscattered radiation originating from the interactions with the calorimeter. It includes charged particles, but also photons and neutrons, back-propagating and generating secondary ionizing particles via their interactions with the upstream material. Particle identification is typically carried out by a precise measurement of its electric charge via a single (or multiple) dE/dx measurement(s) provided by segmented scintillators or by multi-strip/pixel silicon detectors placed at the top of the experimental apparatus. Backscattered (BS) radiation degrades the charge resolution whenever it generates an extra ionization background falling onto the same pixel (or micro-strip, or scintillator element) traversed by the incident CR. It also makes the association of hits to a track more difficult and can downgrade the angular resolution of the tracker. The problem gets worse as the energy of the primary increases.

A traditional approach to the design of charge identifiers is to place them at a reasonable stand-off distance from the calorimeter, optimizing their granularity and performing redundant charge measurements whenever possible. However, this solution requires a large number of readout channels and represents a challenge for the available power budget.

A new approach to strongly mitigate, or even drastically eliminate, this long-standing problem is by exploiting the difference in the time of arrival between the incident particle and the backscattered radiation hitting the detector at a later time. The distance in time Δt between an incident particle traveling with velocity v_{in} and the scattered radiation, back-propagating with an average velocity v_{back} , is proportional to $\Delta t = L(1/v_{in} + 1/v_{back})$, where L is the distance of the detector from the calorimeter. An example is shown in Fig. 2 from a GEANT4 simulation with 1 TeV protons at normal incidence on the calorimeter and a flight path $L=30$ cm (the horizontal axis represents the total flight time in ns). A relativistic particle takes about 1 ns to reach the calorimeter and about as much is taken by the BS radiation to hit the charge detector (while non-relativistic BS particles take >1 ns). Therefore an efficient rejection of the BS background can be achieved with a pixelated instrument with the capability to simultaneously measure the position (x,y,z), charge (q), and timing (t) of the incident particle, effectively acting as a “5D sensor”. In order to maximize the instrument acceptance, a smaller flight path (down to ~ 10 cm) between the charge detector and the calorimeter might be required. In this case time-of-flight measurements have to achieve a sub-ns time resolution. A 10 cm distance corresponds to about 300 ps flight time for relativistic particles to reach the calorimeter and approximately the same amount of time is taken by a relativistic backscatter to reach the top of the instrument. Therefore a ToF instrument with a 100 ps time resolution would allow to reject most of the BS background to better than 5 sigma.

While the requirement on position accuracy is quite severe for spectrometers (e.g., a few micron in the bending plane), the spatial resolution for a calorimeter-based experiment depends on the geometry and design of the instrument. In the case of the MOONRAY telescope, the requirement on the granularity of the CD-ToF instrument is mainly driven by the need to minimize the number of events with a BS hit falling on the same pixel crossed by the incident CR particle. The requirement on the pixel size can then be relaxed, matching the tracker's

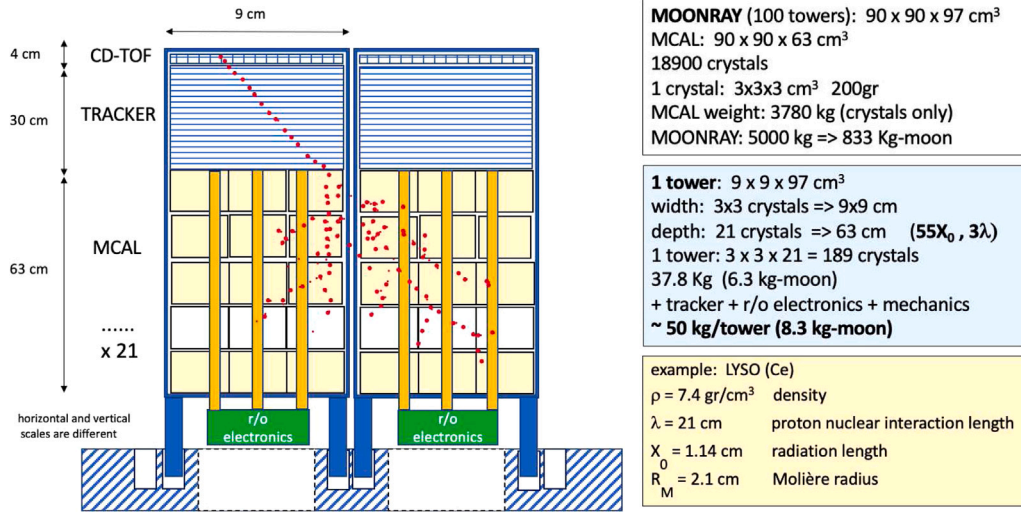


Fig. 1. Conceptual example of two adjacent “towers” approximately 1 m high, 9 cm × 9 cm wide, each weighing ~50 (8.3) kg on Earth (Moon). They are representative of two completely independent modules of the MOONRAY telescope which is structured into 100 towers per m² of active area.

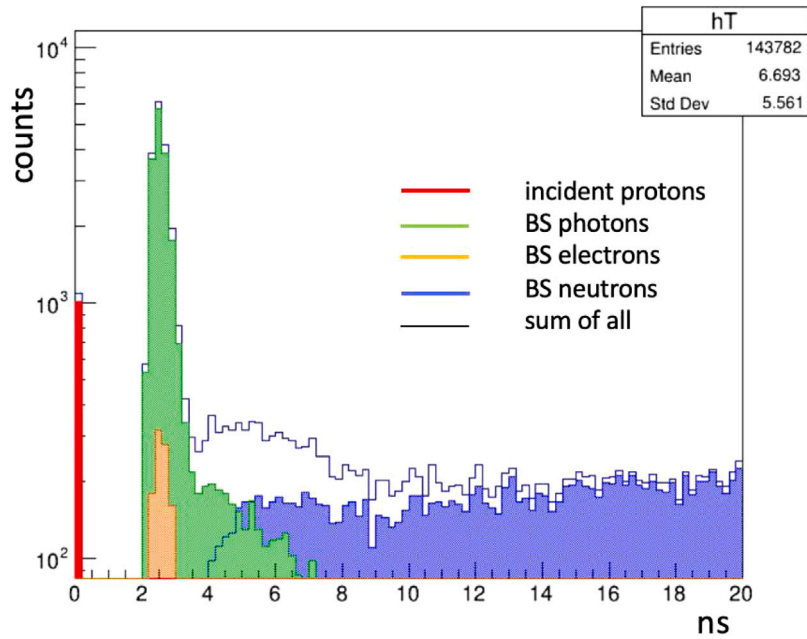


Fig. 2. GEANT4 simulation of BS background generating ionizing secondaries in the charge detector: 1 TeV protons impinging on the calorimeter at normal incidence at time = 0 (red); BS electrons (orange); BS photons (green) generating secondary ionization mostly via Compton scattering; BS neutrons generating ionizing protons (violet); sum of all (unfilled). The horizontal scale is in ns.

resolution on the point-of-impact, down to a few hundred microns or even to O(mm).

Avalanche detectors can achieve a better timing resolution (eventually reaching a few tens ps) than traditional silicon-strip detectors due to the fast rise of the signal (i.e., large slew rate dV/dt) inherent to the avalanche process. Several types of fast and thin avalanche sensors can be implemented as Single Photon Avalanche Diodes (SPADs) or LGADs, with custom segmentation in pixels or strips. However the large Dark Count Rate (DCR) of SPADs, and their intrinsically digital response, are not suitable for our application which requires to operate the detector in a proportional regime to achieve a precision charge

measurement. Therefore, the proposed implementation is focused on pixelated LGADs with a relatively modest internal gain of order 10 and 3 mm granularity. The CD-ToF design is based on two staggered layers of LGAD pixels providing a redundant charge measurement over most of the instrumented area, while ensuring the availability of at least one measurement for particles crossing dead areas in one layer or at the tower boundaries. The details of this geometry, as well as the actual dimensions of the LGAD layers (slightly larger than nominal) are not shown in Fig. 1.

The expected charge resolution of the CD-ToF has been simulated with GEANT4. The energy deposits in the LGAD sensor, generated by

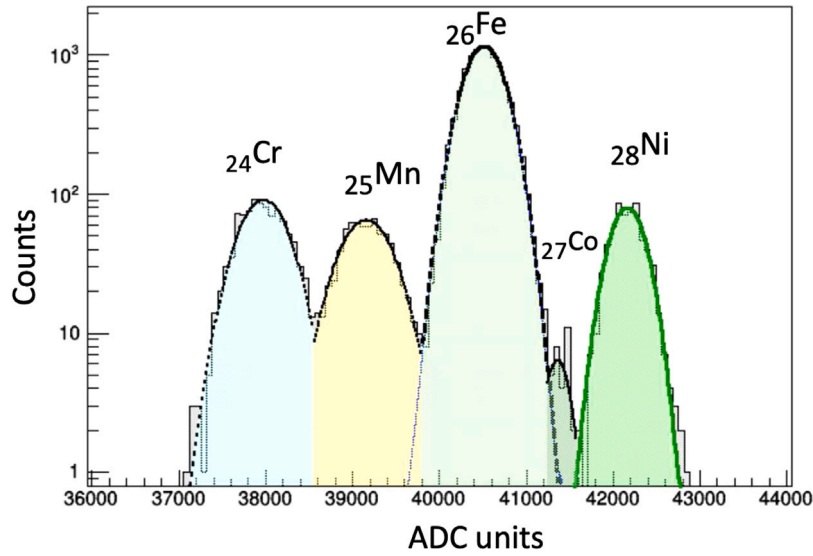


Fig. 3. GEANT4 simulation of charge deposits by ultra-relativistic Mn, Cr, Fe, Co and Ni ions in the CD-ToF, including the response of the LGAD (275 μm thick) and of the front-end electronics. The horizontal scale is in ADC units after digitization of the shaper output signal (16 bits). The relative abundance of the five simulated elements is derived by flight measurements of the iron flux carried out by CALET (see text).

incident ultra-relativistic ions of atomic number $1 \leq Z \leq 40$, is convolved with the parameterized response of the LGAD sensor (based on measurements) and with the simulated noise and linearity of the front-end electronics. At low Z values the charge resolution is dominated by the energy straggling, while the contribution from the electronics noise becomes significant (but sub-dominant) only at $Z > 20$. The charge separation for light ions (e.g., with a charge resolution of ~ 0.1 at proton/helium, ~ 0.15 at boron/carbon) is perfectly adequate to resolve individual elements. For higher charges, an example of the simulated charge distributions is shown in Fig. 3 for the group of elements, with Z from 24 to 28, closest to iron (Mn, Cr, Fe, Co, Ni) whereby their relative elemental abundances are derived from the iron flux measurement by CALET [34] and normalized to iron. The simulated charge resolution at Fe is close to 0.25 (in electron charge units).

The timing resolution of LGAD sensors has been modeled by several authors (including [35,36]) and can be expressed as the quadratic sum of several independent contributions including: jitter, time-walk, Landau noise, signal distortion, and digitization error. The target timing resolution for MOONRAY is 100 ps.

2.2. The tracker sub-module

The gap between the CD-ToF and the calorimeter (MCAL) is instrumented with position sensitive detectors to measure the direction of the incident particle. In the design on the MoonTracker (MT) we can assume that the axis of the shower is reconstructed by the imaging calorimeter, albeit with an angular resolution limited by its coarse granularity, but sufficient to provide a Road-of-Interest (RoI) joining the impact point of the track on the MCAL with the entrance point in the CD-ToF. The latter is cleanly isolated from the BS background (thanks to the ToF rejection) and provides a match with the RoI. A minimum number of 4 coordinates per view from the MT are therefore sufficient to reconstruct the incident track by picking up the genuine track hits along the RoI. The required position resolution is modest (of the order of 150–200 μm) and no additional ToF information is necessary for the MT. With these assumptions, a total of 8 layers of X–Y silicon strip detectors with a readout pitch of 200 μm (e.g., 100 μm pitch with a floating strip) could be implemented with a single wafer per layer for a total of 4000 readout channels per tower. The expected angular resolution is close to 0.1° for C and O nuclei above 10 GeV. The possibility of using thinner sensors (i.e., below 300 μm) to reduce the amount of material budget upstream the calorimeter can be envisaged.

However in this case, a tradeoff between a reduction of the material budget versus the important benefit of a redundant charge identification (provided by 8 independent dE/dx samples in the MT), extending to particles with $Z=1$ with an adequate signal-to-noise ratio, has to be evaluated carefully.

A totally different approach would be the implementation of the MT as a fiber tracker with SiPM readout. However, given the short length of the fibers, one of the main advantages of this kind of detector, namely the reduction in the number of readout channels in the presence of long fibers, would be lost. Also, the saturation of the scintillation light with high Z ions would be detrimental to their charge identification.

2.3. The modular structure of the calorimeter

The CR particle's energy is measured by a homogeneous calorimeter (MCAL) segmented into a 3D array of scintillating cubic crystals, each 3 cm wide. The chosen granularity has to match the Molière radius R_M of the crystal, a parameter governing the transverse lateral development of electromagnetic (e.m.) showers. The requirement of a total longitudinal containment of e.m. showers at TeV energies drives the design value for the depth of the calorimeter to at least $55 X_0$ (radiation lengths). Assuming LYSO(Ce) ($X_0 = 1.14$ cm, $R_M = 2.1$ cm) as the scintillating crystal, each tower would consist of 189 crystals arranged in 21 vertical layers with 3×3 crystals per layer, for a total height of 63 cm (not including spacers) and a weight of 37.8(6.3) kg under Earth (Moon) gravity (see Fig. 1). For a track at normal incidence the total thickness of a tower corresponds to about 3 proton interaction lengths λ_I . The homogeneous calorimeter is designed to meet the requirements of an excellent energy resolution for electrons and positrons and a proton/electron discrimination of 10^5 . The latter is achieved mainly leveraging on the 3D imaging capabilities of the calorimeter, albeit with a granularity of O(cm), and the application of topological cuts based on the different shapes of e.m. versus hadronic showers. Above 100 GeV the energy dependence of the resolution for leptons is expected to level off to a constant term of the order of 1%–2% which ultimately depends on the accuracy in the construction, calibration and stability of the calorimeter. The expected average energy resolution for a baseline design with 100 towers is around 30% for protons with an approximate scaling as $A^{-1/2}$ for nuclei with mass number A . The evaluation of the expected systematic error due to the energy scale uncertainty at the knee is beyond the scope of the present paper. It requires a leap in the present validation of MC code predictions of calorimetric hadronic

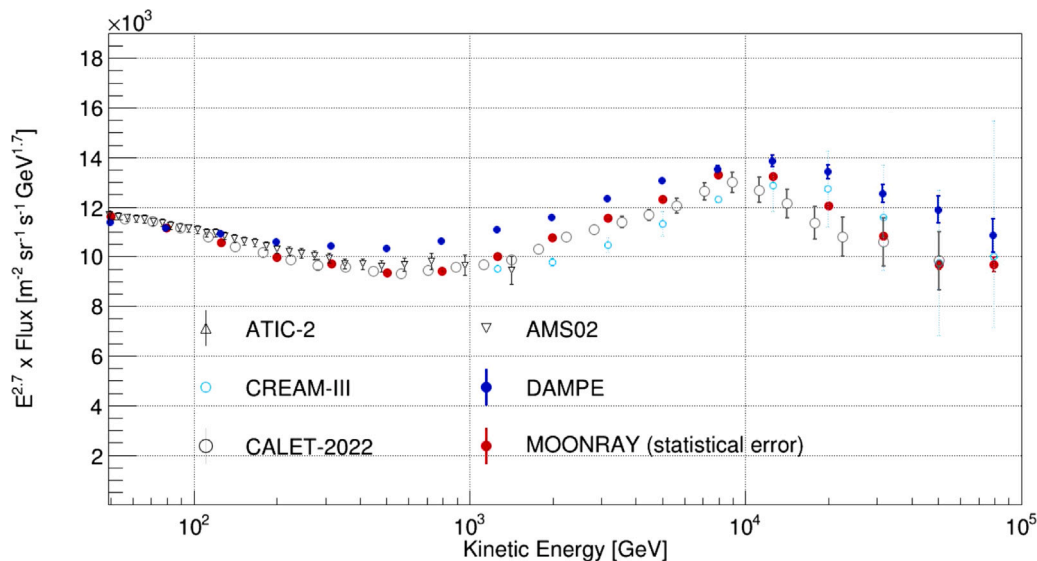


Fig. 4. GEANT4 simulation of MOONRAY proton differential flux (red filled circles) after 5 years of observations and a with a 15×15 towers configuration. Also shown are the measurements by AMS-02, ATIC-2, CREAM-III, CALET and DAMPE. The error bars are representative of statistical errors only.

showers from the scale of O(100 TeV), where direct measurements are available, to the first decade of the TeV scale.

In order to accommodate the huge dynamic range of the calorimetric energy deposits, spanning from a threshold of 0.3 m.i.p. to $\sim 510^6$ m.i.p., each crystal is readout by two photosensors (e.g., photodiodes) of different sensitive area. Each sensor is coupled to multi-range front-end electronics. The readout electronics interface is located at the base of each tower. A telescope with an active area of 1 m^2 would consist of 100 towers arranged in a bi-dimensional array. Special care has to be taken in the design to minimize the amount of inter-crystal gaps and of the passive material at the lateral walls of each tower, while ensuring mechanical stiffness for the insertion or replacement of each unit, and compliance with the allowed eigenfrequency spectrum specified for the launcher.

3. Expected performance and design studies

Preliminary results on the expected performance of MOONRAY, obtained with GEANT4 simulations, indicate that the charge identification capability provided by the CD-ToF allows for a clean separation of individual elements with $Z > 2$ to $Z=28$. This holds even in the most challenging region around iron, as shown in Fig. 3, where the relative abundance of the simulated neighbor elements to iron (Mn, Cr, Co and Ni) is derived from the measurement of the iron flux carried out by CALET [34]. A residual background contamination in the Fe sample of O(1%) is found from the partially overlapping charge distribution of the nearest neighbor (Mn) and O(0.1%) from Cr and Ni, the relative abundance of Co to Fe being very small ($\sim 0.6\%$). A significant improvement is provided by the ToF rejection with respect to the charge separation achieved with the measurements of the iron and nickel fluxes carried out by CALET [34,37] at the highest energy available to date (compare Fig. 3 with figure S1 in the Supplemental Material of [34]). On the side of the lightest elements, the proton Landau tail extends well into the helium distribution, as expected. Despite the reduced level of BS background provided by the ToF rejection, the subtraction of the proton background in the helium sample and the evaluation of its residual systematics will have to rely on the standard analysis procedures adopted, for instance, in [12,13], and [14].

As a case study, a GEANT4 simulation of the expected measurement of the proton flux after 5 years of observations with MOONRAY is shown in Fig. 4 (red filled circles) where it is compared with the presently available experimental points in the energy range from 50 GeV to 100 TeV. The differential proton flux in kinetic energy E is multiplied by $E^{2.7}$. The simulation is based on a MOONRAY configuration with 15×15 towers, corresponding to an active area of about 2.2 m^2 and a geometric factor close to $1.6 \text{ m}^2 \text{sr}$. With the exception of the last bin, the error bar of each point (representative of the statistical error) is smaller than the marker's size, showing a dramatic improvement with respect to the current statistical accuracy of CALET and DAMPE data. This excellent performance is largely driven by the wider (more than one order of magnitude) MOONRAY acceptance, which would allow for a more precise determination of the recently discovered spectral anomalies of proton and helium fluxes and an extension of the measurements into the uncharted region beyond 100 TeV.

At even higher energies, the lessons learned from the unexpected finding of a softening of the proton spectrum observed around 10 TeV tell us that we can only make an educated guess at the value of the proton flux at the PeV scale. In this region, available data are based on ground observations and affected by large systematic errors on the flux and on the elemental composition. While the relative abundance of heavier elements, most notably iron, is expected to become dominant at PeV energies, a direct measurement of the CR composition will require space-borne instruments with an effective acceptance (inclusive of selection cuts efficiencies) of at least $1 \text{ m}^2 \text{sr}$. In this respect, MOONRAY, with its excellent particle identification of nuclei close to iron, is expected to shed light on the elemental composition at the PeV scale.

With the above caveats, an estimate of the flux sensitivity for proton and He above 100 TeV, based on the phenomenological model of [38] and assuming a configuration with 15×15 towers and 10 years of observations, suggests that MOONRAY can bridge the gap from the 100 TeV scale to the knee and establish the elemental composition at the PeV scale with an energy reach to $\sim 2 \text{ PeV}$ with 11 (18) events detected above this energy, respectively. However we must bear in mind that an “energy reach” criterion (e.g., 30% statistical error on the highest bin) is a much easier target than being able to span the energy interval below and above the knee, with direct measurements. Therefore, possible alternatives to the present conceptual design of MCAL are

being studied in order to increase the aspect ratio of the calorimeter, which is the limiting factor for the geometrical factor (GF) of the whole instrument. One of the current ideas under scrutiny is splitting the MCAL into two sub-systems whereby the current homogeneous crystal calorimeter would cover only the first $30 X_0$ and be followed by a more compact “hadronic tail catcher” sampling calorimeter. The rationale is that the upper part of the calorimeter would fulfill the requirements of an electromagnetic calorimeter for the study of the spectrum of electrons+positrons to 20 TeV, while additional $25 X_0$ would be implemented as a sampling calorimeter. The latter can be made roughly $1/3$ shorter than the present lower half of the tower, increasing the GF significantly. Also, an effective resolution of $O(100 \text{ ps})$ for the CD-TOF would allow a similar reduction of the tracker’s total thickness.

4. Conclusions

A conceptual approach towards the design of a lunar CR telescope was elaborated in this paper. The implementation of a multi-ton instrument on the Moon is out of question unless a modular approach is followed. A possible scheme, based on relatively small and lightweight independent modules, is being addressed by the MOONRAY project with the development of the innovative sensors and high energy instrumentation that were briefly introduced in the sections dedicated to the CD-ToF and MCAL.

The scope of this paper is limited to a first conceptual description of MOONRAY as a charged particle telescope. We do not address here important questions related to systematic effects, nor discuss the detection of high energy gamma rays. However we would like to mention two important aspects inherent to the design of the instrument. Firstly, MOONRAY is a pointing instrument allowing for a better control of the time dependence of charged particle fluxes. In fact, for LEO instruments, the latter are integrated over a much shorter orbital period (e.g., 90 min for the ISS) than on the Moon, and affected by latitude variations and magnetic anomalies. Secondly, the CD-ToF system can be used to reject most of the BS background causing fake veto signals in the anti-coincidence systems currently employed for gamma-ray detection.

At the time of writing, the design of the towers is still at a preliminary stage while an active detector R&D development of the LGAD arrays and of the associated front-end electronics is being pursued in Italy in the framework of the activities of the Istituto Nazionale di Fisica Nucleare (INFN).

Declaration of competing interest

The authors declare that they have no known competing financial interests or personal relationships that could have appeared to influence the work reported in this paper.

Data availability

No data was used for the research described in the article.

Acknowledgments

The author would like to acknowledge the support of Istituto Nazionale di Fisica Nucleare for the ongoing development of the CD-ToF sensors and the support of the University of Siena and INFN-Pisa for the computer resources used for the simulations.

References

- [1] A. Panov, et al., *Bull. Russ. Acad. Sci. Phys.* 71 (2007) 494.
- [2] H. Ahn, et al., *Astrophys. J.* 707 (2009) 593.
- [3] M. Aguilar, et al., *AMS-02 Coll.*, *Phys. Rev. Lett.* 115 (2015) 211101.
- [4] M. Aguilar, et al., *AMS-02 Coll.*, *Phys. Rev. Lett.* 119 (2017) 251101.
- [5] M. Aguilar, et al., *AMS-02 Coll.*, *Phys. Rev. Lett.* 120 (2018) 021101.
- [6] M. Aguilar, et al., *AMS-02 Coll.*, *Phys. Rev. Lett.* 121 (2018) 051103.
- [7] Y. Yoon, et al., *Astrophys. J.* 839 (2017) 5.
- [8] E. Atkin, et al., *JETP Lett.* 108 (2018) 5.
- [9] Y.S. Yoon, et al., *CREAM-III Coll.*, *Astrophys. J.* 839 (2017) 5.
- [10] H. Ahn, et al., *Astrophys. J. Lett.* 714 (2010) L89.
- [11] O. Adriani, et al., *Science* 332 (2011) 69.
- [12] M. Aguilar, et al., *AMS-02 Coll.*, *Phys. Rev. Lett.* 114 (2015) 171103.
- [13] O. Adriani, et al., *Phys. Rev. Lett.* 129 (2022) 101102.
- [14] Q. An, et al., *DAMPE, Science Adv.* 5 (2019) eaax3793.
- [15] M. Aguilar, et al., *AMS-02 Coll.*, *Phys. Rev. Lett.* 124 (2020) 211102.
- [16] V. Zatsepin, N. Sokolskaya, *Astron. Astrophys.* 458 (2006) 1.
- [17] A. Vladimirov, G. Jóhannesson, I. Moskalenko, T. Porter, *Astrophys. J.* 752 (2012) 68.
- [18] N. Kawanaka, S. Yanagita, *Phys. Rev. Lett.* 120 (2018) 041103.
- [19] P. Blasi, E. Amato, P.D. Serpico, *Phys. Rev. Lett.* 109 (2012) 061101.
- [20] R. Aloisio, P. Blasi, J. Cosmol. Astropart. Phys. 07 (2013) 001.
- [21] S. Thoudam, J. Hörandel, *Astron. Astrophys.* 567 (2014) A33.
- [22] N. Tomassetti, *Astrophys. J. Lett.* 752 (2012) L13.
- [23] N. Tomassetti, *Phys. Rev. D* 92 (2015) 063001.
- [24] G. Giacinti, M. Kachelrieß, D. Semikoz, J. Cosmol. Astropart. Phys. 07 (2018) 051.
- [25] C. Evoli, P. Blasi, G. Morlino, R. Aloisio, *Phys. Rev. Lett.* 121 (2018) 021102.
- [26] Thoudam, J. Hörandel, *Mon. Not. R. Astron. Soc.* 421 (2012) 1209.
- [27] G. Bernard, et al., *Astron. Astrophys.* 555 (2013) A48.
- [28] P. Lipari, *PoS (ICRC2021)*, Vol. 169, 2021.
- [29] S. Recchia, *PoS (ICRC2021)*, Vol. 168, 2021.
- [30] D. Caprioli, C. Haggerty, P. Blasi, *PoS (ICRC2021)*, Vol. 482, 2021.
- [31] P. Cristofari, P. Blasi, E. Amato, *PoS (ICRC2021)*, Vol. 151, 2021.
- [32] S. Schael, et al., *Nucl. Instr. Methods A* 944 (2019) 162561.
- [33] O. Adriani, et al., *Instruments* 6 (2) (2022) 19.
- [34] O. Adriani, et al., *Phys. Rev. Lett.* 126 (2021) 241101.
- [35] N. Cartiglia, et al., *Nucl. Instr. Methods A* 845 (2017) 47–51.
- [36] G. Giacomini, *Front. Phys.* 9 (2021) 618621, <http://dx.doi.org/10.3389/fphy.2021.618621>.
- [37] O. Adriani, et al., *Phys. Rev. Lett.* 128 (2022) 131103.
- [38] J.R. Hoerandel, *Astropart. Phys.* 19 (2003) 193–220.